ISSN 1349-1148
JAXA-RR-03-012E

JAXA Research and Development Report

Analysis and Experiment on Gas Leakage through CFRP Cross-Ply Laminates under Biaxial Loadings

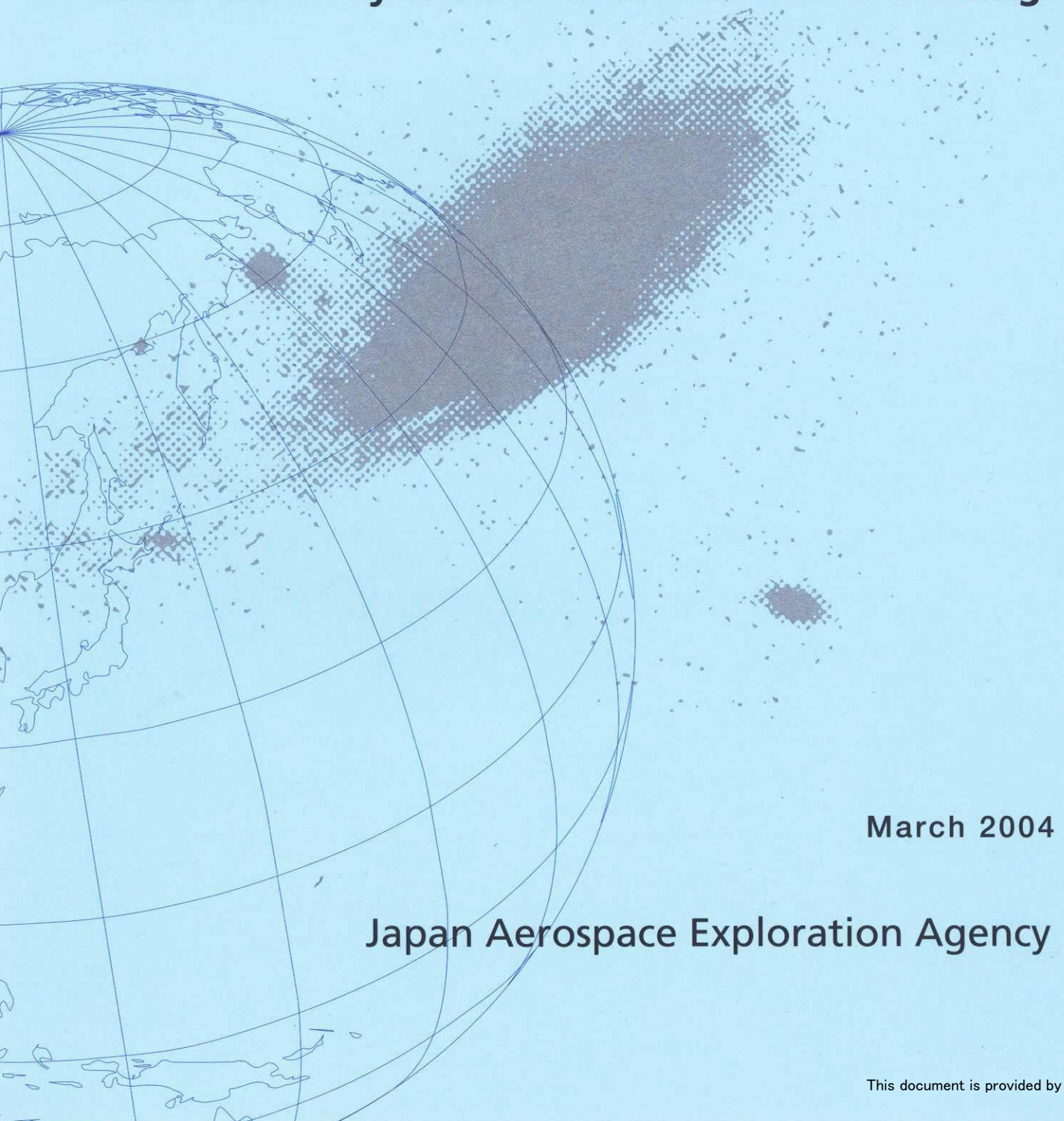

March 2004

Japan Aerospace Exploration Agency

JAXA-RR-03-012E

JAXA Research and Development Report
宇宙航空研究開発機構研究開発報告

Analysis and Experiment on Gas Leakage through CFRP Cross-Ply Laminates under Biaxial Loadings

2軸荷重下におけるCFRPクロスプライ積層板のガス漏洩に関する解析及び実験

Hisashi KUMAZAWA , Takahira AOKI , Ippei SUSUKI
熊澤 寿、青木 隆平、薄 一平

Structure Research Group
Institute of Space Technology and Aeronautics
総合技術研究本部 構造解析研究グループ

March 2004
2004年3月

Japan Aerospace Exploration Agency
宇宙航空研究開発機構

Analysis and Experiment on Gas Leakage through CFRP Cross-Ply Laminates under Biaxial Loadings*

Hisashi KUMAZAWA*1, Takahira AOKI*2, Ippei SUSUKI*1

2軸荷重下におけるCFRPクロスプライ積層板のガス漏洩に関する解析及び実験*

熊澤 寿*1, 青木隆平*2, 薄一平*1

Abstract

It is important to evaluate gas leakage through composite laminates due to the existence of matrix cracks for the purposes of a substantial weight reduction in reusable rockets by the application of CFRP (carbon fiber reinforced plastic) composite to propellant tanks. In this study, the leak properties through CFRP cross-ply laminates under biaxial loadings were investigated. Leak analysis for damaged CFRP laminates has been developed based on the opening displacements of matrix cracks acting as leakage paths. The leak rate through the damaged laminates under biaxial loading was measured in an experiment using cruciform specimens at room temperature. Calculations of the leak rate based on the leak analysis coincided well with experimental results, showing the leak rate to be closely dependent on crack openings in the laminates. Numerical results indicate that an increase in propellant leakage can be caused by the enlargement of crack opening displacements due to mechanical and thermal loads, increase of crack density and decrease of temperature.

Keywords: composite material, CFRP laminate, matrix crack, permeability, propellant leakage, cruciform specimen, biaxial loading, cryogenic tank

概　　要

発展型使い捨てロケットや再使用型ロケットなどの性能向上において、複合材料製推進剤タンクによる軽量化が不可欠である。極低温推進剤の低温環境における内圧や構造荷重、製造時の微小欠陥などが原因となりマトリックスクラックが発生した場合、マトリックスクラックにより引起される推進剤漏洩が非常に問題となる。本研究では、CFRP(carbon fiber reinforced plastic)複合材料が損傷した場合の漏洩特性についての解析および実験を実施した。内部に損傷のあるクロスプライ積層板の漏洩解析を、クラックの開口に基づき定式化を行った。また、平板十字型試験片を用いた２軸荷重下におけるヘリウムガス漏洩試験を常温にて実施し、CFRP積層板が損傷した場合の漏洩特性を測定した。漏洩解析による数値計算結果は実験結果とよく一致し、本研究で定式化したクラックの開口に基づく漏洩解析の有効性が示せた。漏洩特性の数値解析結果から、損傷の増大、温度の低下、負荷によるマトリックスクラックの開口が漏洩を増大させることが明らかとなった。

1 Introduction

Carbon fiber reinforced plastics (CFRP) tanks are expected to be utilized in several fields for the advantage of reduced weight. For reusable launch vehicles (RLV), particularly single stage launchers, weight reduction of propellant tanks, which represent a large part of the structural mass, are of high priority and may be attained with the use of CFRP

* Received 6 February 2004 (平成16年2月6日受付)

*1 Structure Research Group (構造解析研究グループ)

*2 University of Tokyo (東京大学)

composites. Recent studies[1,2] pointed out that the cryogenic temperature of liquid hydrogen affects the properties of CFRP materials and induces severe thermal strains. One of the major consequences is the initiation of matrix cracks at relatively low loads even in the toughened CFRP laminates. The accumulation of matrix cracks not only influences mechanical performance of the structures but may also lead to propellant leakage through the laminate tank walls.[3] Other experimental studies revealed that the existence of matrix cracks in the CFRP laminate could cause large leak rate compared to the permeation due to diffusion.[4-7] However, analytical investigations of leakage for these CFRP laminates have not yet been pursued.

The objective of this study is to clarify the mechanism of the through-thickness propellant leakage of CFRP cross-ply laminates due to the existence of chains of matrix cracks. In this study, the leakage through CFRP laminates is experimentally investigated with the use of small test specimens instead of costly full- or sub-scale tanks. An analytical formulation is developed based on the simple modeling that there is a relationship between leakage and opening displacements of matrix cracks. Leak experiments using cruciform specimens are conducted to acquire experimental data. Constants used in the leakage analysis are determined by the experimental results under uniaxial loadings, and then leak rates under biaxial loadings are calculated with these constants and compared with the experimental results. The comparison shows that the numerical calculations are in good agreement with the experimental results, and crack opening displacements have close relationship with leakage. The leak analysis is proved to be capable of calculating the leak behavior under mechanical loading including biaxial tension. In addition, the influences of matrix crack density and temperature on leakage are numerically evaluated based on the leak analysis.

2 Gas Leak Analysis

The gas permeation through a laminate is composed of two mechanisms, diffusion and leak. Gas diffusion is the phenomenon that takes place when the gas atoms diffuse into the materials and pass through the laminate. In the case of leakage, gas flows through the leak path that consists of continuously connected matrix cracks in each layer(cascade of matrix cracks), that result in a sequence of connecting passages between both sides of the laminate. If there are layers without cracks in the laminate, leakage doesn't take place and diffusion alone is present. Generally, the permeation due to diffusion is negligible compared to that due to leakage through leak paths.[8] In this paper, the permeation implies leakage and the effects of diffusion are negrected. The analytical scheme presented here is based on the assumption of leakage from one side of the laminate surface to the other, through the cascade of matrix cracks developed in each ply of the laminate.[9]

2.1 Modeling

Leak rate which is the quantity of mass flowing through leak paths per second can be expressed in several units of measure. In vacuum engineering, the product of pressure and volume per second is used as unit of measure. Leak rate Q ($Pa\ m^3 / s$) for compressible gas is expressed as the product of volumetric flow rate Q_V (m^3 / s) and pressure P (Pa) at specified temperature.

$$Q = P \cdot Q_V \qquad (1)$$

The mass flow rate can be recalculated from leak rate using Eq. (A6) in Appendix A. In this paper, leak rate Q is converted the value per unit area of a laminate and the unit of leak rate is the product of pressure and volume per the product of unit area and unit time ($Pa\ m^3 / m^2 / s$).

In this model, it is postulated that cracks exist in each component ply of the laminate, and that these cracks act as leak paths connecting both sides of the laminate. Therefore, the basic assumption for leakage is that the leak rate Q is governed by the overall conductance that can be derived from the combination of the multiple cracks in the laminate. The flow rate per unit area Q ($Pa\ m^3 / m^2 / s$) is expressed in terms of the overall conductance C

(m^3 / m^2 / s) and the pressure difference ΔP (Pa) between the two laminate surfaces that represents the driving force of the leakage, and thus Q is in the form,[10]

$$Q = C\Delta P \qquad (2)$$

In the case of compressible gas, the volumetric flow rate does not represent the quantity of gas flow unless the pressure and temperature are specified.

The overall through-the-thickness conductance C is derived from the combined sum of intra-ply conductances through matrix cracks and inter-ply conductances at each crack intersection between two matrix cracks in adjacent layers. Based on the strictly theoretical crack model, the two adjacent cracks at an intersection have no overlapping area. However, the microscopic interface defects at an overlapping region of two matrix cracks in adjacent layers are assumed to provide the connecting path between the matrix cracks as shown in Fig. 1. The matrix crack intersection point and its surrounding area of the matrix cracks in the interlaminar regions are assumed to play major role in affecting the leakage level, acting as the throats in the leakage path. The rest of the portions of the opened cracks, including the above mentioned intra-ply path, have relatively little effect on the leak rate of the entire laminate, and thus their effects on leakage are neglected herein.

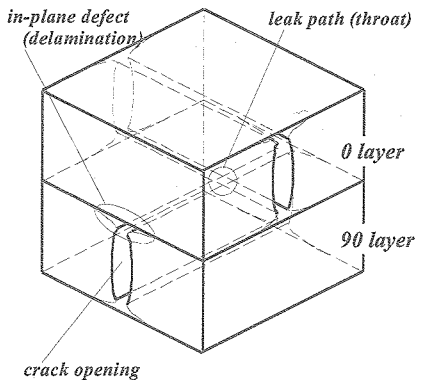

Fig. 1 Leak path at intersection of two matrix cracks.

Following the theory of vacuum engineering for molecular flow, conductance through an orifice is proportional to the orifice area $A_{orifice}$ and root mean square velocity of molecules $\sqrt{3RT/M}$ where R is the gas constant, T is the absolute gas temperature and M is the molecular weight[10]. The orifice conductance $c_{orifice}$ can be expressed as follows

$$c_{orifice} \propto A_{orifice}\sqrt{T/M} \qquad (3)$$

Crack openings adjacent to an intersection would widen the throat area. It is assumed that the throat at a crack intersection performs as an orifice, and the throat area is proportional to the product of crack opening displacements in adjacent layers. Thus the throat area A_k at the intersection of cracks between k-th layer and $(k+1)$-th layer in the cross-ply laminate (Fig. 2) is described as

$$A_k \propto \overline{\Delta}_k \overline{\Delta}_{k+1} \qquad (4)$$

where $\overline{\Delta}_k$ is a mean opening displacement of cracks in k-th layer. The conductance c_k through the throat area A_k at a crack intersection is derived from Eqs. (3) and (4) as follows

$$c_k = \Omega_M(T)\overline{\Delta}_k \overline{\Delta}_{k+1} \qquad (5)$$

$$\Omega_M(T) = \Omega\sqrt{\frac{T}{T_{R.T.}}\frac{M_{helium}}{M}} \qquad (6)$$

where $\Omega_M(T)$ ($m^3/m^2/s$) is the proportionality factor for an operating gas with molecular weight M at specified temperature T, $T_{R.T.}$ is the room temperature(25°C), M_{helium} is the molecular weight of helium(=4), and Ω ($m^3/m^2/s$) is the proportionality factor for helium gas at room temperature(25°C) ($=\Omega_{Mhelium}(T_{R.T.})$). Constant Ω is generally dependent on thickness of layers and shape of interface defects at the intersection of matrix cracks. Constant Ω for helium gas at room temperature is experimentally determined in the present study. Ω is assumed to be a constant throughout the laminate in consideration for approximation to avoid a complex formulation.

The number of intersection points between *k-th* and *(k+1)-th* layers in a unit area is $d_k d_{k+1}$, where d_k is a crack density of *k-th* layer. Conductance between *k-th* and *(k+1)-th* layers per unit area $\bar{c}_k$ is thus written with c_k as

$$\bar{c}_k = d_k d_{k+1} c_k \tag{7}$$

Using reciprocal formula for series conductance, conductance through the whole laminate C is obtained as

$$C = \left(\sum_k \frac{1}{\bar{c}_k} \right)^{-1} \tag{8}$$

The conductance and the leak rate through the whole laminate are derived from Eqs. (2), (5), (6), (7) and (8) as follows

$$C = \Omega \sqrt{\frac{T}{T_{R.T.}} \frac{M_{helium}}{M}} \left(\sum_k \frac{1}{d_k d_{k+1} \bar{\Delta}_k \bar{\Delta}_{k+1}} \right)^{-1} \tag{9}$$

$$Q = \Omega \sqrt{\frac{T}{T_{R.T.}} \frac{M_{helium}}{M}} \left(\sum_k \frac{1}{d_k d_{k+1} \bar{\Delta}_k \bar{\Delta}_{k+1}} \right)^{-1} \Delta P \tag{10}$$

Leak rate Q is obtained as a function of crack densities, opening displacements of matrix cracks and pressure difference. In this study, matrix crack densities are enumerated from ultrasonic C-scan. The conventional two-dimensional shear-lag analysis for the cross-ply laminate (Appendix B) is applied to the calculation of mean crack opening displacements $\bar{\Delta}_k$, which are dependent on mechanical strains caused by applied load and thermal strains caused by a decrease in temperature from the initial stress-free temperature. Knowing the initial stress-free temperature and assuming a constant Ω are important in calculating the leak rate, because initial temperature is one of the determining factors for calculation of the crack opening displacement. Initial stress-free temperature of CFRP laminates is not exactly equal to the curing temperature due to the existence of stress relaxation, and it is therefore difficult to determine the initial temperature appropriately. Therefore, constant Ω and initial temperature are determined based on the experimental leak data in the present study.

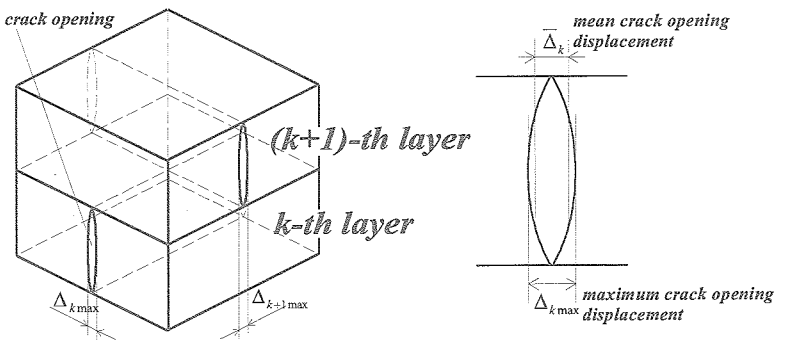

Fig. 2 Intersection of two matrix cracks and crack opening displacements.

2.2 Influences of Constant Ω and Initial Stress-Free Temperature

Leak rate in Eq. (10) is dominantly characterized by constant Ω and analytically calculated crack opening displacement $\bar{\Delta}_k$ in each layer, which is a function of thermal strains and applied stresses(Eq. (B9) in Appendix B). Constant Ω and initial stress-free temperature denoted as T_0 make different contributions to the calculation of leak rate. The calculated result under the range of Ω and T_0 is illustrated by the following examples. In these examples, crack density is assumed to be constant

regardless of temperature and stress for apparent characterization of these constants, and mean crack opening displacement $\overline{\Delta}_k$ in the case that coefficient of thermal expansion remains unchanged irrespective of temperature, is expressed as Eq. (B10) in Appendix B. Leak rates are normalized as the values under unit volume at atmospheric pressure and room temperature per unit second from Eq. (10) and Eq. (A7) in Appendix A as follows

$$Q_{V,RT,ATM} = \Omega\sqrt{\frac{T_{R.T.}}{T}\frac{M_{helium}}{M}}\left(\sum_k \frac{1}{d_k d_{k+1}\overline{\Delta}_k\overline{\Delta}_{k+1}}\right)^{-1}\frac{\Delta P}{P_{ATM}} \tag{11}$$

Leak rates calculated as functions of temperature under the conditions of fixing one of the parameters, T_0 or Ω, are shown in Fig. 3 (a) and (b). Figure 3 shows that leak rate increases as temperature lowers mainly due to the enlarged crack opening displacements caused by the increased thermal contraction. Moreover, coefficient $1/\sqrt{T}$ in Eq. (11) add to the leak rate increase at lower temperature. The decrease in temperature has the effect of increasing the leak rate. Figure 3 (a) indicates the effect of Ω, in which the leak rate curve is magnified proportionally at each temperature. The effect of T_0 shown in Fig. 3 (b) is represented by the shift of the leak rate curve parallel to temperature because leak rates are functions of temperature difference $(T - T_0)$ since the mean crack opening displacement $\overline{\Delta}_k$ in Eq. (B10) is a linear function of temperature difference.

Figure 4 indicates the effects of Ω and T_0 on leak rate at specified temperature under compressive and tensile stresses for the case of uniform biaxial stresses $\sigma_X = \sigma_Y$. In this paper, x and y axes coincide with 0° and 90° directions of laminates respectively, and z axis is the direction of the ply thickness. In Fig. 4, closure of matrix cracks due to compressive stress leads to a decrease of leak rate, and *vice versa*. In Fig. 4 (a), Ω magnifies the leak rate proportionally as in Fig. 3 (a), and leak rates calculated with different Ω_1 and Ω_2 vanish at the same compressive stress since the crack opening displacement $\overline{\Delta}_k$ in Eq. (11) vanishes at given stress irrespective of the value of Ω. The crack opening displacement $\overline{\Delta}_k$ (Eq. (B10)) is a function of mechanical stress and thermal stress, and if initial temperature T_0 increases, thermal stress gets larger and shifts the leak rate curve parallel to the stress axis as shown in Fig. 4 (b).

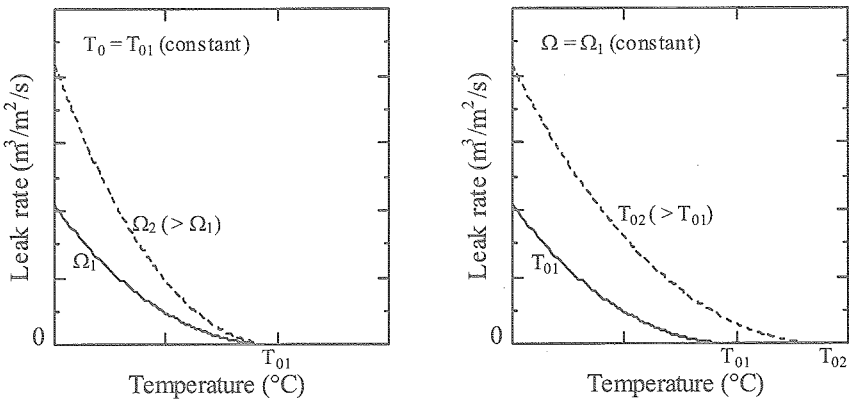

(a) T_0 = constant (b) Ω = constant

Fig. 3 Effects of constants Ω and T_0 on leak rate under varying temperature without loading.

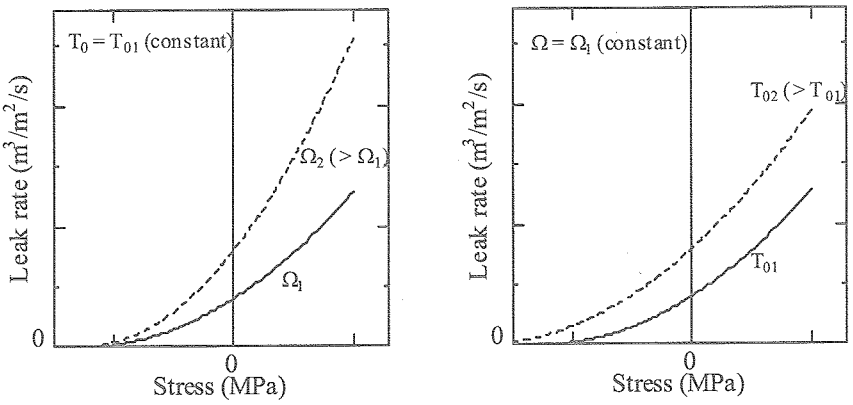

(a) T_0 = constant (b) Ω = constant

Fig. 4 Effects of constants Ω and T_0 on leak rate under varying stress.

Calculated leak rates under given stress and temperature increase in either case when Ω or T_0 increases, and constants Ω and T_0 cannot be determined by measured leak rate under a single condition of specific stress and temperature. It is requisite for determination of constants Ω and T_0 to acquire leak rates varying in association with temperature or stress. For example, the way to determine constants Ω and T_0 on the basis of leak rates measured as functions of stress at room temperature is outlined below. Crack opening displacement in Eq. (B9) and leak rate in Eq. (10) are functions of biaxial stresses σ_X and σ_Y at room temperature, and rewritten as $\overline{\Delta}_k(\sigma_X, \sigma_Y)$ and

$$Q(\sigma_X,\sigma_Y)=\Omega\sqrt{\frac{M_{helium}}{M}}\left(\sum_k \frac{1}{d_k d_{k+1}\overline{\Delta}_k(\sigma_X,\sigma_Y)\overline{\Delta}_{k+1}(\sigma_X,\sigma_Y)}\right)^{-1}\Delta P \qquad (12)$$

From Eq. (12), $Q(\sigma_X, \sigma_Y)/Q(0, 0)$ is independent of constant Ω as follows

$$\frac{Q(\sigma_X,\sigma_Y)}{Q(0,0)}=\frac{\left(\sum_k \frac{1}{d_k d_{k+1}\overline{\Delta}_k(0,0)\overline{\Delta}_{k+1}(0,0)}\right)}{\left(\sum_k \frac{1}{d_k d_{k+1}\overline{\Delta}_k(\sigma_X,\sigma_Y)\overline{\Delta}_{k+1}(\sigma_X,\sigma_Y)}\right)} \qquad (13)$$

Measured leak rate divided by that with stress free is compared with $Q(\sigma_X, \sigma_Y)/Q(0, 0)$ calculated for several tentative initial temperatures on a graph, and suited value for T_0 can be determined to adjust the shape of the $Q(\sigma_X, \sigma_Y)/Q(0, 0)$ curve to measured data. Subsequently, Ω's are resolved to quantitatively match $Q(0, 0)$ under previously determined initial temperature T_0 to measured leak rate without loading.

3 Experimental Procedure

3.1 Biaxial Test for Cruciform Specimen

A biaxial testing machine consists of four hydraulic actuators of 250kN(tension/compression) capacity each for static and fatigue loads. These four actuator assemblies make two pairs, and are rigidly mounted in an octagonal box-shaped frame diagonally (Fig. 5). Each loading axis is called x- and y-axis, which coincide with 0° and 90° directions of a laminate respectively in this research. The

frame is of heavy-duty welded construction, and placed horizontally. Available testing space in the machine is about 1000 mm×1000mm.

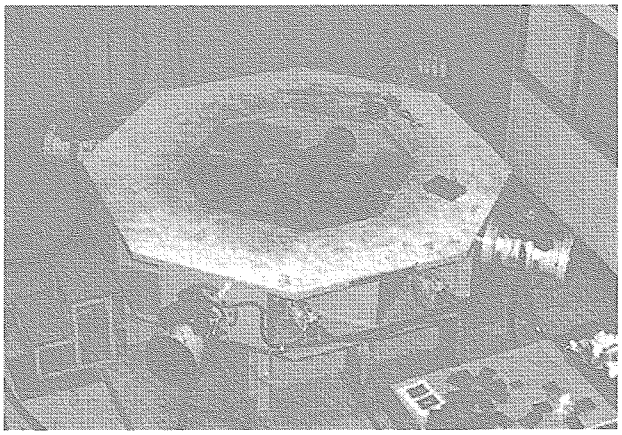

Fig. 5 Biaxial testing machine.

The material systems used in this study were carbon fiber/180°*C* cured epoxy IM600/#133 (Vf=0.6) and IM600/#101(Vf=0.55). The laminates with stacking sequence of $(0°/0°/90°/90°)_S$ were fabricated as the cruciform specimens. GFRP (glass fiber reinforced plastic) tabs were bonded on the laminate, and the geometry of cruciform specimens for leak test is shown in Fig. 6. IM600/#133 and IM600/#101 specimens were labeled as SPECIMEN A and SPECIMEN B respectively. The effect of material system on the constant Ω can also be acquired by comparing the results for the different materials. The thickness of the leak test area of the specimens was about 1.2 mm. Applied loads to the cruciform specimen in x(0°) and y(90°) directions are defined as F_X and F_Y.

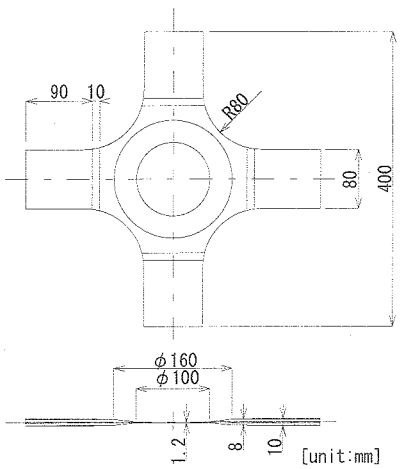

Fig. 6 Cruciform specimen for leak test.

Because of the ring reinforcement around the gauge area, stresses in the center portion of specimen are unable to calculate directly. So it is important to comprehend the strains induced by the biaxial loads in the gauge area for calculating the stresses. Gauge area for leak measurement is 45mm × 45mm on the center of biaxial specimen as shown in Fig. 7. Strains had been measured with strain gauges on the gauge area to the maximum of the strain range of 0.2%, in which no damage occurred on the laminate. Then, the relationships between biaxial loads and strains were acquired before leak test. The strain gauges were detached from the cruciform specimen after the strain measurements.

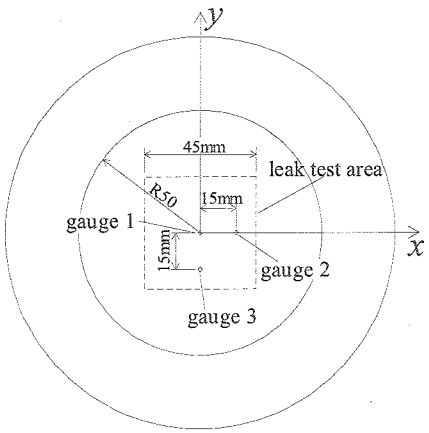

Fig. 7 Gauge area for leak test and strain gauges on the central portion on specimen.

3.2 Detection of Damage and Leakage

Prior to leak experiments, two specimens were subjected to biaxial loads for several cycles to induce matrix cracks at room temperature as shown in Tables 1 and 2. It is necessary to obtain the matrix crack density in the laminates for evaluating the effect of the damage on leakage. X-ray photography is widely adopted for observation of the damage inside composite materials. However, the penetrant of X-ray photography infiltrated in the matrix cracks might obstruct the accurate measurement of permeability. Then ultrasonic C-scan was carried out to observe the growth of matrix cracks in the CFRP laminate after loading. The results of the C-scan were obtained using a through transmission with a glass reflector plate, and a 25MHz transducer was used to emit and receive the ultrasonic energy.

The ultrasonic C-scan with reflector plate records the ultrasound that passes through the specimen, reflects off a flat glass plate, and passes back through the specimen to the transducer(Fig. 8). The amplitude of the ultrasonic signal returning to the transducer is very sensitive to physical changes, e.g. matrix crack, in the laminate.

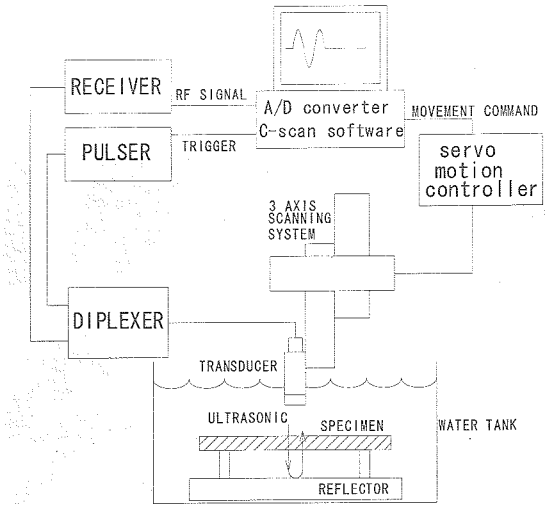

Fig. 8 Schematic of the ultrasonic C-scan set-up.

Table 1 Applied loads and strains to SPECIMEN A before leak test.

Cycle	Fx MAX (kN)	Fy MAX (kN)	εx MAX (%)	εy MAX (%)	load speed:Fx (kN/min)	load speed:Fy (kN/min)
1	79.9	38.1	0.61	0.18	75.0	35.8
2	50	100	0.24	0.76	37.5	75.0

Table 2 Applied loads and strains to SPECIMEN B before leak test.

Cycle	Fx MAX (kN)	Fy MAX (kN)	εx MAX (%)	εy MAX (%)	load speed:Fx (kN/min)	load speed:Fy (kN/min)
1	62	32	0.47	0.16	75.0	38.7
2	30.4	60.4	0.15	0.46	37.7	75.0
3	40	77	0.20	0.58	39.0	75.0
4	40.2	80.5	0.19	0.61	37.5	75.0

Ultrasonic inspections from both sides, right-side and back-side, of a specimen were conducted to ascertain whether the crack in 0° direction appeared on C-scan is in right-side or back-side $[0°]_2$ layer. The cracks in $[0°]_2$ layer on under surface appear sharper than those on the top surface due to dead band on the front face. The results of ultrasonic C-scan to observe the matrix cracks in the laminate are compared with one of X-ray photography for confirmation, and this ultrasonic C-scan technique turns out to be an effective method for damage detection for CFRP laminates. The matrix cracks in the leak test area (45mm × 45mm) of the two specimens were thus inspected as shown in Fig. 9. Figure 9 also indicates that matrix cracks exist in $[90°]_4$ layers and $[0°]_2$ layer on both sides of $(0°/0°/90°/90°)_S$ laminates after loading. The continuous series of these matrix cracks through all layers provoke the leak path through the laminate. Matrix crack densities of the laminates were enumerated from Fig. 9, and used to calculate leak rates in the leak analysis.

The leak measurement system consists of two stainless steel cups for gas supply and leak capture, a helium leak detector and a recorder for permeability and biaxial loads data as shown in Fig. 10, and is capable to measure permeability through the planar laminate. Two stainless steel cups are padded on the laminate as shown in Fig. 11, and fixed on the center portion of the cruciform specimen with using a frame(Fig. 12). Helium gas is fed to the laminate surface from gas container, and flow at very low rate through the gas supply cup to keep atmospheric pressure inside the cup. The detection cup entraps leakage gas through the laminate specimen in the gauge area, and the helium leak detector connected to the detection cup measures the permeability. Contact area between the two cups and the laminate are sealed by O-rings to avoid undesirable leakage as shown in Fig. 11. Helium gas that leak through the laminate can be captured concurrently with applying loads to the cruciform laminate(Fig. 13), and it is possible to vary biaxial load level and their ratio quasistatically during the leak measurement.

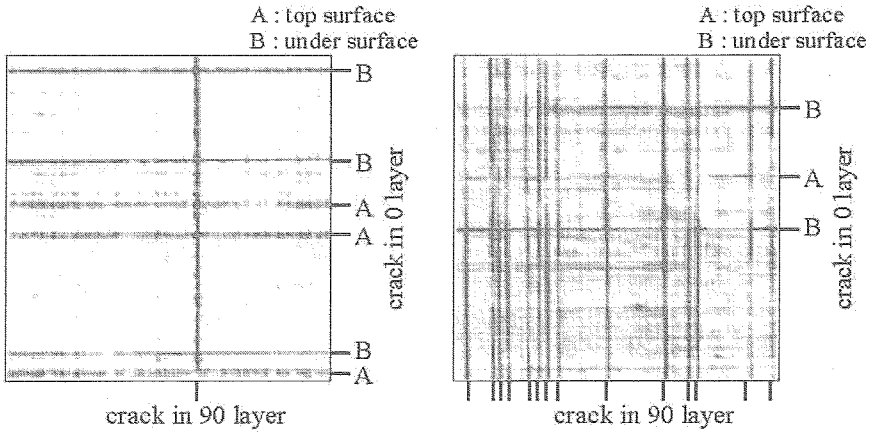

(a) SPECIMEN A (IM600/#133) (b) SPECIMEN B (IM600/#101)

Fig. 9 Matrix crack accumulation in leak test area (45mm × 45mm) of $(0/0/90/90)_S$ laminates.

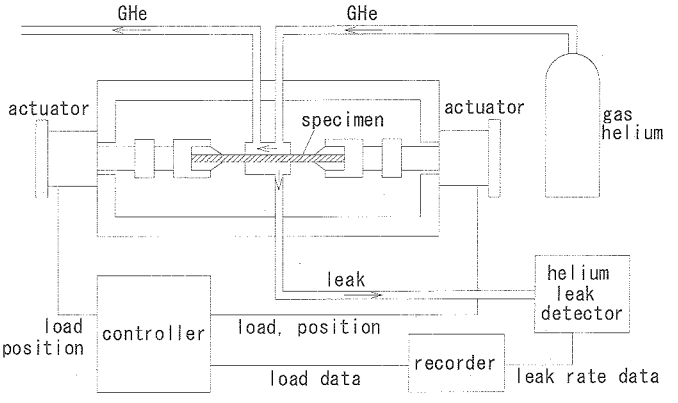

Fig. 10 Leakage measurement system for cruciform specimen under biaxial loading.

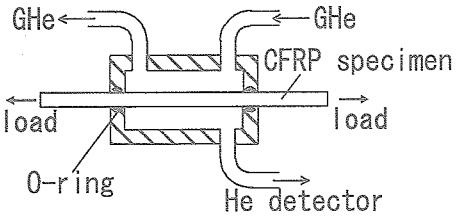

Fig. 11 Schematic view of apparatus for leak rate measurement.

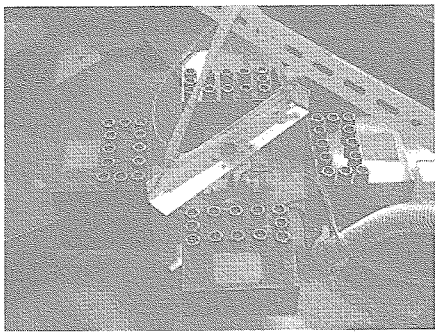

Fig. 12 Photograph of leak test under biaxial loading.

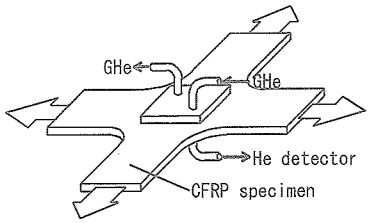

Fig. 13 Leak experiment through a laminate under biaxial loading.

4 Results and Discussion

The numerical and experimental results are compared for assessment of the validity of the leak analysis developed in the present study. The leak analysis requires the determination of an appropriate constants Ω and T_0. Hence the verification sequence starts with determination of the constants according to measured leak data of cruciform laminates under uniaxial load for each material. Then leak rate through the laminate under biaxial load is calculated with thus determined Ω and T_0, and compared with measured leak rate. In the calculation of leak rate, the anisotropic elastic constants and thermal expansion coefficients of IM600/#133 (SPECIMEN A) are treated as dependent on temperature as presented in Fig. 14.[1] In the results, leak rates are converted to the values under unit volume at atmospheric pressure and room temperature per second through the use of Eq. (A7) in Appendix A.

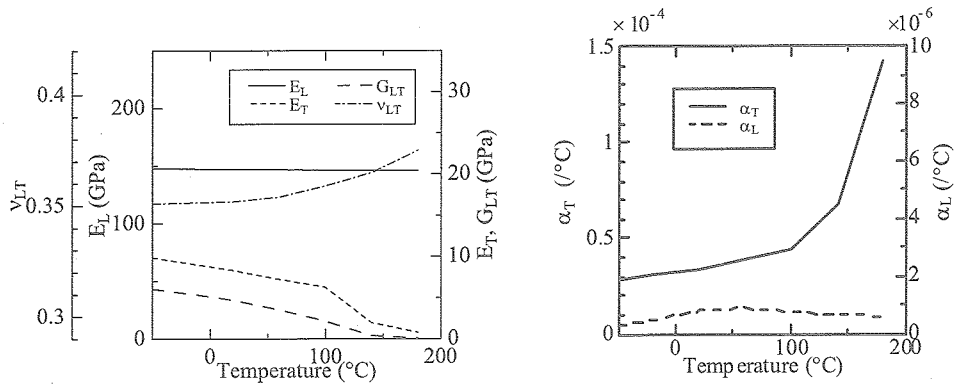

(a) Elastic constants (b) Thermal expansion coefficients

Fig. 14 Temperature dependent material constants of IM600/#133.

4.1 Comparison between Leak Analysis and Experiment

The method to determine constants Ω and T_0 with Eq. (13) is applied and the comparison between numerical and experimental results is shown in Fig. 15. Leak rates are calculated numerically with varying initial temperatures. Leak rates through the cruciform laminate under uniaxial load are experimentally measured at room temperature. Numerical calculation of the leak rate is conducted with initial temperature T_0 from 80°C to 120°C at 10°C intervals, and constant Ω for each initial temperature that is determined by comparing the calculated leak rate and corresponding measured value under zero mechanical loads (ε_x=0). Though numerical results under uniaxial load do not vary with respect to the direction of the uniaxial loading, experimental results show different measured leak rates under different loading direction (Fig. 15). For the symmetric property of the stacking sequence $(0°/0°/90°/90°)_S$ and boundary conditions on the middle surface and the external surface, the mean opening displacements of cracks in $[0°]_2$ and $[90°]_4$ layers under biaxial stresses, $\overline{\Delta}_0(\sigma_X, \sigma_Y)$ and $\overline{\Delta}_{90}(\sigma_X, \sigma_Y)$, have the relationship as follows (Eq. (B11) in Appendix B)

$$\overline{\Delta}_0(\sigma_1,\sigma_2) = \overline{\Delta}_{90}(\sigma_2,\sigma_1) \tag{14}$$

And $\overline{\Delta}_0(\sigma_X, \sigma_Y) \times \overline{\Delta}_{90}(\sigma_X, \sigma_Y)$ is identical under the two conditions, $(\sigma_X, \sigma_Y) = (\sigma_1, \sigma_2)$ and (σ_2, σ_1) derived from Eq. (14) as follows

$$\overline{\Delta}_0(\sigma_1,\sigma_2)\times\overline{\Delta}_{90}(\sigma_1,\sigma_2) = \overline{\Delta}_0(\sigma_2,\sigma_1)\times\overline{\Delta}_{90}(\sigma_2,\sigma_1) \tag{15}$$

Thus the calculated leak rate $Q(\sigma_X, \sigma_Y)$ in Eq. (12), which is a function of $\overline{\Delta}_0(\sigma_X, \sigma_Y) \times \overline{\Delta}_{90}(\sigma_X, \sigma_Y)$, have no difference irrespective of load direction from Eq. (15).

$$Q(\sigma_1,\sigma_2) = Q(\sigma_2,\sigma_1) \tag{16}$$

Under the present assumption of leakage model, the leak analysis has been developed with neglecting the intra-ply conductance through the cracks in

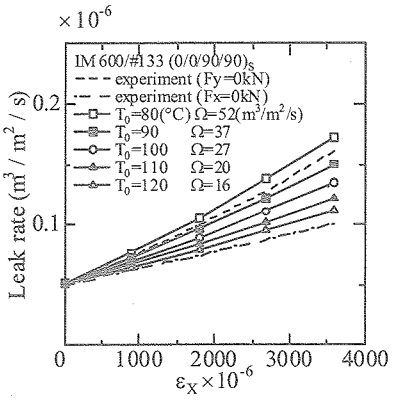

Fig. 15 Comparison between measured and analytical leak rates under uniaxial load (SPECIMEN A).

$90°_4$ layer, which is a function of $\overline{\Delta}_{90}(\sigma_X, \sigma_Y)$. In the experimental results, change in the intra-ply conductance through matrix cracks in $90°_4$ layer could have lead to the difference between two measured leak rates under different load directions as

$$Q(\sigma_1,\sigma_2) \neq Q(\sigma_2,\sigma_1) \tag{17}$$

It is unachievable for the leak analysis for $(0°/0°/90°/90°)_S$ laminates under the present assumption to obtain the numerical results dependent on the direction of uniaxial load. Thus the constants are determined to accommodate the calculated leak rate with the least difference from two experimental results for different load directions concurrently.

Suitable constants are selected for the leak rate curve lying between the measured leak rates under uniaxial load in $x(0°)$-direction and $y(90°)$-direction. Figure 15 indicates that the calculated leak rates under condition of initial temperatures ranging from 90°C to 110°C are approximately suitable for the measured leak rates through the laminate SPECIMEN A submitted to uniaxial load. Ω ranges from 20 $m^3/m^2/s$ to 37 $m^3/m^2/s$ with temperature from 90°C to 110°C. Though value of Ω is responsive to small change of initial temperature, T_0 =100°C and Ω=27 $m^3/m^2/s$ are used as representative values in the calculation for leak rate. In a similar way, the constant Ω for SPECIMEN B was determined as a representative value by comparing calculated leak rates with experimental results as shown in Table 3. In this determination procedure, material properties

of IM600/#101 are assumed to be identical to those of IM600/#133, since the two CFRP materials consist of 180°C cured epoxy resin and identical carbon fiber, both of which dominantly determine the material constants.

Table 3 reveals that the constant Ω for SPECIMEN A is lower compared to that for SPECIMEN B. Constant Ω in Eqs. (5) and (6), which indicates the likelihood of gas passage at the crack intersection, can easily be surmised to be affected by the extent of interface damage at an overlapping region of cracks. It can be deduced that Ω for SPECIMEN A is lower than that of SPECIMEN B, since the microscopic delamination at the crack intersection in toughened material SPECIMEN A would be smaller than that in SPECIMEN B. The difference of damage level may also have been caused by the conditions of loading. Strain free initial temperature is not necessarily equal to curing temperature, but seems to be much lower than the latter. The 4mm GFRP tabs were bonded to the 1.2mm thick laminate specimens on both sides with thermosetting adhesive films as shown in Fig. 6. Fall in temperature from curing temperature of adhesive films (120°C) supposedly induces compression in the gauge area of specimens due to large thermal contraction of the GFRP tabs compared to that of the CFRP gauge area at room temperature.

Table 3 Constants Ω and T_0 for $(0/0/90/90)_S$ laminates.

Specimen	Material	Ω ($m^3/m^2/s$)	T_0 (°C)
A	IM600/#133	27	100
B	IM600/#101	44	100

Numerical calculations for the two CFRP laminates, of which matrix crack densities are different as shown in Fig. 9, are compared with experimental results in Fig. 16. This figure shows the measured leak rates of SPECIMEN A and SPECIMEN B under biaxial load ratios $F_Y/F_X = 1$ ($\varepsilon_y/\varepsilon_x$=1) and $F_Y/F_X = 0$ ($\varepsilon_y/\varepsilon_x$=-0.2), together with the numerical results using Ω's determined from uniaxial load test. The numerical calculations are in very good correlation with the experimental results in Fig. 16. The leak rate through the laminate in the case of a biaxial strain ratio $\varepsilon_y/\varepsilon_x$=1 is larger than that in case of strain ratio $\varepsilon_y/\varepsilon_x$=-0.2. This enhancement of leakage implies that the amount of crack opening displacements under strain ratio $\varepsilon_y/\varepsilon_x$=1 are larger than those under strain ratio $\varepsilon_y/\varepsilon_x$=-0.2, and in consequence conductance of leak path composed of cracks becomes relatively higher. Figure 16 indicates that the biaxial stress level and their ratio have a great impact on the leak rates.

4.2 Numerical Examples

Leak rates are calculated by Eq. (11) to clarify the effect of crack density, biaxial stresses and temperature on gas leakage for the IM600/#133 (0°/0°/90°/90°)s laminates. The constant Ω = 27 $m^3/m^2/s$ and initial temperature $T_0 = 100°C$ are assumed in the subsequent calculations.

Leakage through the laminate with no mechanical load at room temperature as function of crack density is shown in Fig. 17. In this figure, matrix crack densities in $0°_2$ and $90°_4$ layers (d_0 and d_{90}) are assumed to be equal. Leak rate increases in accordance with increasing amounts of matrix cracks because parallel leak paths grow in number.

The effect of crack density and stress on the leak rate is shown in Fig. 18. In this figure, the leak rates are calculated under the condition of crack density d_0 ($=d_{90}$) = 0.5, 1.0 /cm and stress ratio of $\sigma_Y/\sigma_X = 0$, 1 at room temperature for illustration. Figure 18 shows that not only the crack density but also the load levels and their ratio affect the leakage. The leak rate under biaxial stresses σ_Y/σ_X =1 is larger than that under uniaxial stress σ_Y/σ_X =0 due to the difference in crack opening displacements.

Leak rate as function of temperature under no mechanical load is calculated and shown in Fig. 19. Crack densities d_0 and d_{90} are assumed to remain unchanged as the temperature is lowered. The decrease of temperature results in the increase of leak

rate, which is due to the enlargement of crack opening displacements caused by the thermal contraction and the temperature effect on velocity and density of molecules.

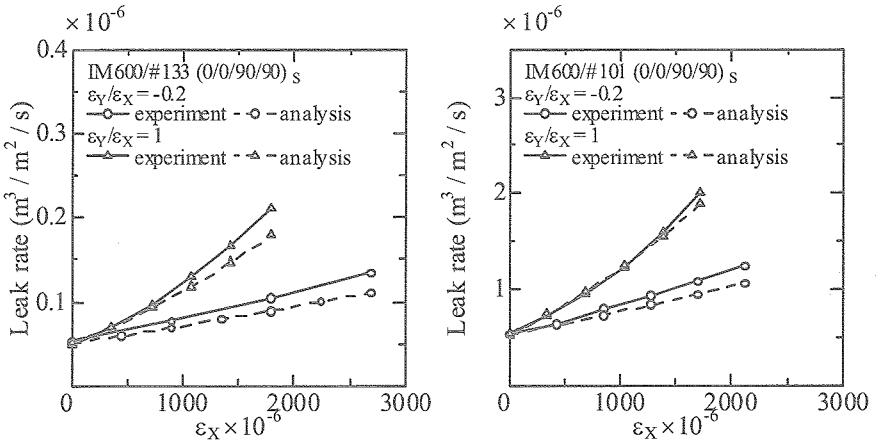

(a) SPECIMEN A (IM600/#133) (b) SPECIMEN B (IM600/#101)

Fig. 16 Comparison between measured and analytical leak rates through $(0/0/90/90)_S$ laminate.

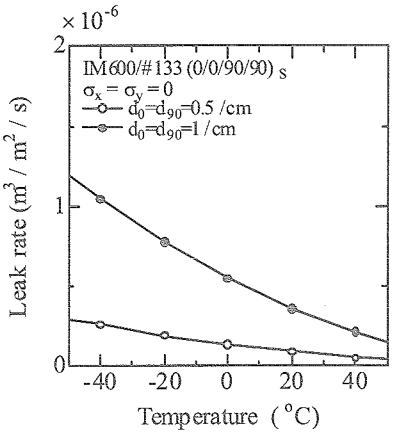

Fig. 17 Relationships between calculated leak rate and crack density through IM600/#133 $(0/0/90/90)_S$ laminate with no mechanical load.

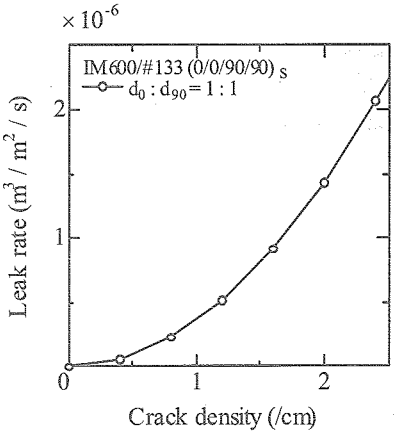

Fig. 18 Increase of calculated leak rate through IM600/#133 $(0/0/90/90)_S$ laminate under biaxial stresses.

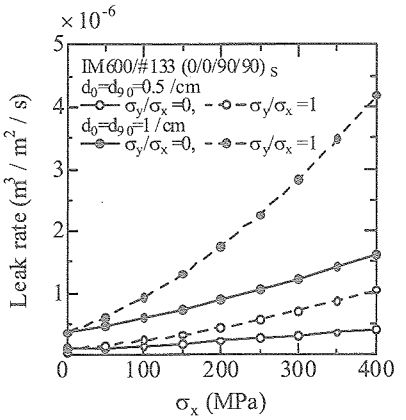

Fig. 19 Relationships between temperature and calculated leak rate through IM600/#133 $(0/0/90/90)_S$ laminate with no mechanical load.

5 Conclusions

To clarify the mechanism of propellant leakage through damaged carbon fiber reinforced plastics cross-ply laminates, leak analysis based on the opening displacements of matrix cracks has been developed. In leak analysis, conductance at the crack intersection in the laminate acting as a throat of the leak path is assumed to be proportional to the product of opening displacements of matrix cracks in adjacent layers, based on the analogy with the molecular flow through an orifice. Permeability of the whole laminate has been derived from the combined sum of the conductance at the intersection of matrix cracks, and numerical calculations are in good agreement with experimental results, which have been acquired from the leak tests through laminates with matrix cracks at room temperature. The leak analysis in this study is based on a simple assumption of a relationship between conductance and crack opening, and can be used to evaluate the influence of mechanical and thermal loads on propellant leak through carbon fiber reinforced plastics cross-ply laminates. The results of this study also indicate that the leak characteristics at the intersection of matrix cracks would depend on the expansion of the microscopic defects in the vicinity of the crack intersections, and the enlargement of crack opening displacements due to mechanical and thermal loads has a great impact on the gas leakage.

Appendix A
Unit Conversion for Leak Rate

Ideal gas law is written as follows,[11]

$$P = nkT \tag{A1}$$

$$n = N / V \tag{A2}$$

$$k = mR / M \tag{A3}$$

where

P : pressure
n : concentration of molecules
k : Boltzmann's constant
T : absolute temperature
N : number of molecules
V : volume
m : mass of a molecule
R : gas constant
M : gram molecular weight

Ideal gas law is rewritten from Eqs. (A1)-(A3) as follows,

$$\frac{PV}{T} = \frac{w}{M} R = const. \tag{A4}$$

where w is the weight of gas($=mN$). The relationship between volumetric flow rate Q_V (m^3/s) and mass flow rate Q_W (g/s) is obtained from Eq.(A4) as follows,

$$\frac{PQ_V}{T} = \frac{Q_W}{M} R \tag{A5}$$

Mass flow rate Q_W (g / s) is obtained using R ($Pa\ m^3/g\ mole\ K$), T (K) and M ($g / mole$) from Eqs. (1) and (A5) as

$$Q_W = Q \cdot \frac{M}{RT} \tag{A6}$$

Leak rates in the analysis and experiment in this paper are converted to the value under unit volume at atmospheric pressure and room temperature per second ($Q_{V,RT,ATM}$ (m^3/s)) from Eqs. (1) and (A5) with constancy of Mass flow rate Q_W

$$Q_{V,RT,ATM} = \frac{1}{P_{ATM}} \frac{T_{R.T.}}{T} Q \qquad \text{(A7)}$$

where $T_{R.T.}$ (K) is the room temperature and P_{ATM} (Pa) is the atmospheric pressure.

Appendix B
Crack Opening Displacements Based on Two-Dimensional Shear-Lag Analysis

Shear lag analysis for calculation of crack opening displacements in $(0_n/90_m)_S$ cross-ply laminates subjected to in-plane tensile stresses σ_x and σ_y, are formulated based on the assumption of deformations of cracked layers.[12] In this analysis, the cross-ply laminates are assumed to have symmetric stacking sequence such as $(0_n/90_m)_S$. x and y axes coincide with 0° and 90° directions respectively, and z axis is the direction of the ply thickness. The ply thicknesses of 0° and 90° layers are denoted as $2t_0$ and t_{90} respectively, and the matrix cracks in the laminate are assumed to be uniformly spaced along the x- and y-directions at Dx and Dy intervals as shown in Fig. B1.

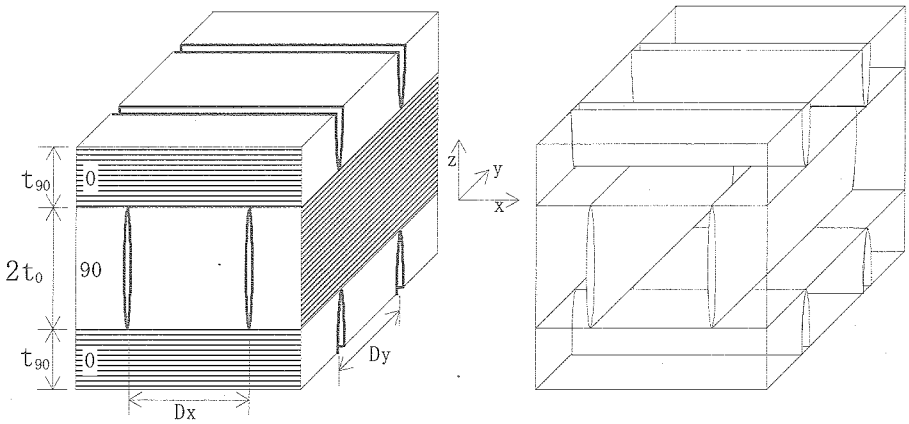

Fig. B1.Crack geometry used for modeling in cross-ply laminate.

Crack opening displacements are considered to be of quadratic functions in the thickness direction, and x- and y-directional displacements u and v in the laminate are assumed to be

$$u = u^{90} + \frac{z^2}{t_{90}^2}(u^0 - u^{90}) \quad (-t_{90} \le z \le +t_{90}) \qquad \text{(B1)}$$

$$v = v^{90} \quad (-t_{90} \le z \le +t_{90}) \qquad \text{(B2)}$$

$$u = u^{90} \qquad (t_{90} \le |z| \le t_{90} + t_0) \qquad \text{(B3)}$$

$$v = v^0 + \frac{(z - t_0 - t_{90})^2}{t_0^2}(v^0 - v^{90}) \quad (t_{90} \le |z| \le t_{90} + t_0) \qquad \text{(B4)}$$

where u^0, v^{90}, u^{90} and v^0 are functions of coordinates x and y.

The shearing stresses at 0° /90° interface τ_{xz}^{90i} and τ_{yz}^{90i} are derived from Eqs. (B1)-(B4), with assumptions of $\partial w/\partial x \approx 0$ and $\partial w/\partial y \approx 0$ (w is z-directional displacement), as

$$\tau_{xz}^{90i} = \frac{2G_{23}}{t_{90}}(u^0 - u^{90}) \qquad \text{(B5)}$$

$$\tau_{yz}^{0i} = \frac{2G_{23}}{t_0}(v^0 - v^{90}) \qquad \text{(B6)}$$

where G_{23} is the out-of-plane shear modulus of a ply.

Solving the equilibrium equations together with Eqs.(B5) and (B6), the constitutive equations and boundary conditions, the average stresses in 0° layer σ_x^0 and σ_y^0 are obtained as follows

$$\sigma_x^0 = A_x \cosh(R_x x) + B_x \cosh(R_y y) + K_x \qquad \text{(B7)}$$

$$\sigma_y^0 = A_y \cosh(R_x x) + B_y \cosh(R_y y) + K_y \qquad \text{(B8)}$$

where A_i, B_i, R_i and K_i (i=x, y) depend on geometrical and damage parameters, elastic constants, applied stresses and initial strains. A_i, B_i and K_i (i=x, y) are linear functions of applied stresses and initial strains, and thus the average stresses σ_x^0 and σ_y^0 are linear functions of applied stresses and initial strains. Similarly average stresses in 90° layer σ_x^{90} and σ_y^{90} have the same linearity.

Crack opening displacements in Eqs. (B1)-(B4) are also the linear functions of applied stresses and initial strains as the strains are linear combinations of stresses, which are linear functions of applied stresses and initial strains. Then average crack opening displacements $\overline{\Delta_0}$ and $\overline{\Delta_{90}}$, which are calculated from quadratic crack opening displacements, can be expressed as x- and y-directional average stresses ($\overline{\sigma_x}$ and $\overline{\sigma_x}$) and longitudinal and transverse thermal strains (ε_{10} and ε_{20}) of the laminate as follows,

$$\overline{\Delta_i}(\overline{\sigma_x},\overline{\sigma_y},\varepsilon_{10},\varepsilon_{20}) = H_{iA}\overline{\sigma_x} + H_{iB}\overline{\sigma_y} + I_{iA}\varepsilon_{10} + I_{iB}\varepsilon_{20} \quad (i=0,90) \qquad \text{(B9)}$$

where H_{ij} and I_{ij} (j =A, B) are constants.

In particular, average crack opening displacements $\overline{\Delta_0}$ and $\overline{\Delta_{90}}$ are the functions of applied stresses and temperature difference ($T - T_0$) when coefficients of thermal expansion are constant,

$$\overline{\Delta_i}(\overline{\sigma_x},\overline{\sigma_y},T) = H_{iA}\overline{\sigma_x} + H_{iB}\overline{\sigma_y} + I_i(T-T_0) \quad (i=0,90) \qquad \text{(B10)}$$

where I_i is a constant.

In this paper, the above analysis was applied to the $(0°/0°/90°/90°)_S$ cross-ply laminates. Coefficients in Eq. (B9) in the case that crack spacings in 0° and 90° layers are equal or adequately large, have following relationships due to the symmetrical conditions of material constants and geometry of laminates as shown in Fig. B2.

$$H_{0A} = H_{90B} \ , \ H_{0B} = H_{90A} \ , \ I_{0A} = I_{90A} \ , \ I_{0B} = I_{90B}$$

Then average crack opening displacements in 0° and 90° layers satisfy the following equation.

$$\overline{\Delta_0}(\sigma_1,\sigma_2,\varepsilon_{10},\varepsilon_{20}) = \overline{\Delta_{90}}(\sigma_2,\sigma_1,\varepsilon_{10},\varepsilon_{20}) \qquad \text{(B11)}$$

In Eq. (B11), crack opening displacements are symmetric with respect to biaxial stresses for the laminate used in this paper.

Acknowledgments

The author acknowledges Yoichi Hayashi from Tokyo Business Service and Takashi Ishikawa from Advanced Composite Evaluation Technology Center for their invaluable contributions to this research.

References

1) Aoki, T., Ishikawa, T., Kumazawa, H. and Morino, Y., "Cryogenic Mechanical Properties of CF/Polymer Composite for Tanks of Reusable Rockets," Advanced Composite Materials, Vol.10, No. 4 (2001) pp. 349-356.
2) Schoeppner, G. A., Kim, R. and Donaldson S. L., "Steady State Cracking of PMCS at Cryogenic Temperatures," AIAA paper 2001-1216.
3) "Final Report of the X-33 Liquid Hydrogen Tank Test Investigation Team," (2000) NASA Marshall Space Flight Center.
4) Okada, T., Nishijima, S., Fujioka, K. and Kuraoka, Y., "Gas Permeation and Performance of an FRP Cryostat," Advances in Cryogenic Engineering, Vol. 34 (1988) pp. 17-24.
5) Disdier, S., Rey, J. M., Pailler, P. and Bunsell, A. R., "Helium Permeation in Composite Materials for Cryogenic Application," Cryogenics, Vol.38,

No. 1 (1998) pp. 135-142.
6) Rivers, H. K., Sikora, J. G., and Sankaran, S. N., "Detection of Hydrogen Leakage in a Composite Sandwich Structure at Cryogenic Temperature," Journal of Spacecraft and Rockets, Vol. 39, No. 3 (2002) pp. 452-459.
7) Robinson, M. J., Eichinger, J. D. and Johnson, S. E., "Hydrogen Permeability Requirements and Testing for Reusable Launch Vehicle Tanks," AIAA paper 2002-1418.
8) Kumazawa, H., Aoki, T. and Susuki, I., "Modeling of Propellant Leakage through Matrix Cracks in Composite Laminates," AIAA paper 2001-1217.
9) Kumazawa, H., Aoki, T. and Susuki, I., "Analysis and Experiment of Gas Leakage through Composite Laminates for Propellant Tanks," AIAA Journal, Vol. 41, No. 10 (2003) pp. 2037-2044.
10) Holkeboer, D. H. and Pagano, F., Jones, D. W. and Santeler, D. J., "Vacuum Engineering," (1967) pp. 83-116, Boston Technical Publishers.
11) Holkeboer, D. H. and Pagano, F., Jones, D. W. and Santeler, D. J., "Vacuum Engineering," (1967) pp. 23-28, Boston Technical Publishers.
12) Henaff-Gardin, C., Lafarie-Frenot, M. C. and Gamby, D., "Doubly Periodic Matrix Cracking in Composite Laminates Part 1: General In-Plane Loading," Composite Structures, Vol. 36, No. 1-2 (1996) pp. 113-130.

JAXA Research and Development Report
(JAXA-RR-03-012E)

Date of Issue : March 25, 2004

Edited and Published by :
Japan Aerospace Exploration Agency
7-44-1 Jindaiji-higashimachi, Chofu-shi,
Tokyo 182-8522 Japan

Printed by :
BCC Co., Ltd.
2-4-1 Hamamatsu-cho, Minato-ku, Tokyo 105-6114 Japan

Japan Aerospace Exploration Agency